Progress In Electromagnetics Research M, Vol. 112, 81–91, 2022

Design and Analysis of a Mid-Infrared Ultra-High Sensitive Sensor Based on Metal-Insulator-Metal Structure and Its Application for Temperature and Detection of Glucose

Hocine Bensalah[1, 2, *], Abdesselam Hocini[1], and Hocine Bahri[3]

Abstract—In this paper, a compact and highly sensitive refractive index plasmonic sensor, based on a metal-insulator-metal (MIM) waveguide coupled to double hexagonal ring-shaped resonators in the mid-infrared range, is proposed and analyzed using the finite-difference time-domain (FDTD) method embedded in the commercial simulator R-soft, where it has been found that the transmission peaks and dips positions can be easily manipulated, by simply adjusting the structural parameters of the proposed design, such as the inner side length and the distance between the centers of the two hexagonal ring resonators. So, these parameters have a key role in the sensor's performances, and it is clearly noticed from the results, where a linear link between the refractive index of the material under testing and its wavelength resonances was established. Furthermore, the maximum achievable linear sensitivity was $S = 4074\,\text{nm/RIU}$, with a matching sensing resolution of $2.45 \times 10^{-6}\,\text{RIU}$; the temperature sensitivity is around $1.55\,\text{nm/°C}$; and the highest linear sensitivity is $S = 3910\,\text{nm/RIU}$ in 0–200 g/L glucose concentration, making this proposed sensor an attractive one, to be implemented in high-performance nano and bio-sensing devices.

1. INTRODUCTION

Classical optical sensing systems, when it comes to the implementation in a compact, miniaturized, and highly integrable environment, and they are not a feasible solution, because photonic devices are larger in size than their electrical counterpart, because of the diffraction limit of the light. This led to a quest for a more practical alternative method, therefore plasmonic sensor structures [1].

Plasmonic based structures have been extensively employed to circumvent this discomfort, due to their unique capabilities in light directing and management below the diffraction limit, and attributing to the employment of surface plasmon polariton (SPP).

The influence of an input electromagnetic field in a continuous dielectric media frees electrons in metal, generating an exciting SPP based wave, with a focused energy in nanoscale scale, consequently, circumventing the optical diffraction limit problem [2].

Sensors, filters, lasers, and many other devices have been proposed using the SPP phenomena, such as the proposed sensor in [3], where the authors proposed a Si nano-ring located inside a circular cavity, acting both as an optical sensor and a notch filter, and as for the authors of [4], they have used a graphene nanoribbon material on a Fabry-Perot resonator (FPR) sensor to enable mid-infrared applications. In [5], the authors proposed a fast-tunable filter on a curved graphene surface by means of a plasmonic guided wave resonance, and many more other optical devices were also designed and based

Received 26 March 2022, Accepted 22 June 2022, Scheduled 26 July 2022

* Corresponding author: Hocine Bensalah (hocine.bensalah@univ-msila.dz).

[1] Laboratoire d'Analyse des Signaux et Systèmes, Department of Electronics, University of M'Sila, BP. 166, Route Ichebilia, M'sila 28000, Algeria. [2] Université Yahia Fares Médéa, Médéa, Algeria. [3] Laboratory of Electronics and New Technologies (LENT), University Oum El Bouaghi, Algeria.

on the SPP phenomena, such as the couplers in [6], the photo detector in [7], and the optical switches in [8], in addition to the logical gates in [9, 10], and the perfect plasmonic absorbers in [11] and [12].

Mid-infrared region (MIR) is recently attracting great attention due to the wide range applications. These applications include; thermal imaging, industrial applications, infrared spectroscopy, health-related fields, chemical and biological sensing [13, 14]. The importance of this spectral region arises from the fact that many chemical and biological molecules have their characteristic absorption within this region [15]. Optical detection of molecules is based on intensity or wavelength change due to change in the real or imaginary part of the analyte refractive index [16]. Both imaginary and real parts of the refractive index, of the molecules under detection, exhibit a peak around its characteristic absorption wavelength, hence amplifying the effect that is detected by the optical device. This fact makes mid-infrared region a suitable range for biomolecular and gas detection with high sensitivity.

However, most of the presented plasmonic structures are based on silver which has significant constraints in the MIR band due to the lack of SPP confinement to the silver surface in the MIR [17].

Metal-insulator-metal (MIM) waveguides are one of the most basic plasmonic waveguide structures, where light is confined within a considerable propagating space. This attracted the attention of many researchers, and they have been employed in numerous applications. MIM based plasmonic sensors and filters are one of the most innovating devices in optical circuits and have been investigated numerically and experimentally, such as the nanodisk resonators [18], tooth-shaped waveguide [1], the ring resonators [19], and the racetrack resonators [20].

Although there have been a lot of studies on different plasmonic MIM waveguides, the interactions of incident MIR waves with tunable MIM waveguides have been less researched. The MIR spectrum contains wavelengths spanning from 2 to 20 µm, reflecting the molecular fingerprint zone, and prospective MIR applications have been extensively described in various studies. In particular, plasmonic MIM waveguide sensors are essential for an air transparent window of the MIR spectrum from 2 to 12 µm [21]. Therefore, there are still many efforts in this subject that need to be undertaken [22, 23].

Sensitivity is one of the most significant components in analyzing the performance of a sensor, where it is vital to have a better sensitivity by simply using various geometrical topologies. In addition to that, the resonance wavelengths can be adjusted according to the geometrical modifications of the ring resonator-based design, such as the one proposed here.

In this work, a double intersected hexagonal shaped ring resonator coupled to a metal-insulator-metal based waveguide is proposed as a refractive index nano-sensor. It is simulated and analyzed using the finite-difference time-domain (FDTD) method, where the perfectly matched layer (PML) boundary condition is imposed. Structural parameters were varied to study their effects on the sensor's performance, such as the distance between the center of the two intersected hexagonal ring resonators and their inner side length, and the results are shown in the last section with their corresponding discussions, followed by a conclusion on the matter at hand.

2. THE STRUCTURE AND THEORETICAL ANALYSIS

The proposed MIM based plasmonic sensing structure is composed of two identical and intersected hexagonal rings with a slit, as shown in Fig. 1, where all structural parameters are illustrated accordingly, i.e., the spacing between the hexagonal shaped ring resonator and the waveguide, the width of this latter, the height between the two ring centers, and the distance separating the two ring centers, which are g, w, H, and D, respectively, alongside the inner and outer side lengths L_2 and L_1.

Fixing the waveguide's width to 50 nm leads to the (TM) being the only excited mode in the MIM based waveguide [3]. The dielectric material and silver layer are represented in our structure by the white and gray areas, respectively.

The silver's frequency dependent dielectric constant is expressed by Lorentz-Drude model as follows [24]:

$$\varepsilon_m(\omega) = \varepsilon_\infty - \frac{\omega_p^2}{\omega(\omega + i\gamma)} \tag{1}$$

where $\varepsilon_\infty = 3.7$ is the dielectric constant at the infinite angular frequency; ($\omega_p = 1.38 \times 10^{16}$ rad/s) is the bulk plasma frequency; γ is the electron collision frequency ($\gamma = 2.73 \times 10^{13}$ rad/s); and ω is the

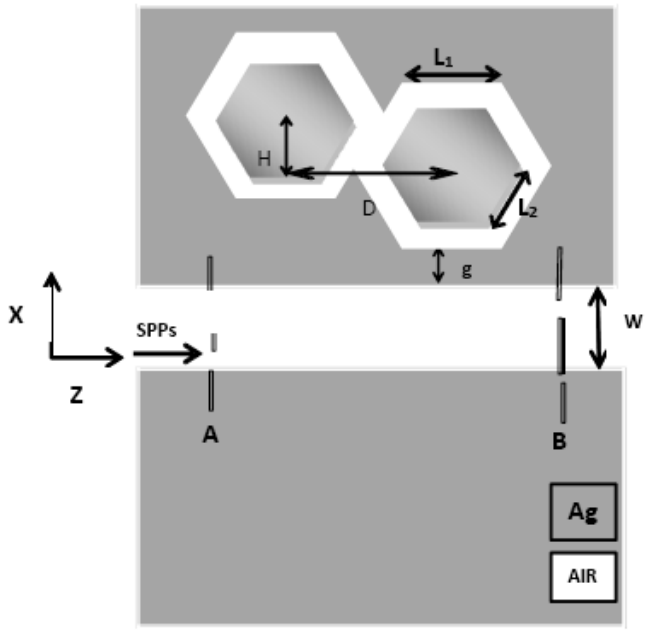

Figure 1. The schematic diagram of the proposed MIM based plasmonic structure.

incident wave's angular frequency in vacuum [25].

Since the incident light of the SPP mode excitation is of a TM-polarized nature, the magnetic field in our simulation process is set to be parallel to the y axis [12].

A single hexagonal shaped plasmonic based cavity's resonance wavelength can be approximately obtained using the following [26]:

$$\lambda_m = \frac{\mathrm{Re}(n_{eff}) \times (6L_{eff})}{m - \varphi 2\pi}, \tag{2}$$

where L_{eff} and $\mathrm{Re}(n_{eff})$ are the hexagonal cavity's effective side lengths and the real part of the effective refraction index, respectively, and m is a positive integer which represents the standing SPP wave's order in the cavity; φ denotes the total phase shift in the corners of the hexagonal cavity.

By using the FDTD method embedded in the commercial simulator R-soft [27], where the Perfectly Matched Layers (PML) condition is applied as the absorbing boundary of the outgoing waves, our proposed structure is then simulated, and its transmission characteristics are analyzed, by taking into account the grid size of $\Delta x = \Delta z = 3\,\mathrm{nm}$, in both the x and z directions. The transmitted input type was a TM polarized continuous Gaussian modulated wave and was collected at the other end of the waveguide. It is defined as $T = P_{out}/P_{in}$, where P_{in} and P_{out} are the incident and transmitted powers, observed at the two positions A and B, respectively.

One of the most important aspects and parameters that describes how well a surface plasmon resonance (SPR) based sensor performs is sensitivity (S). It is defined as Δ_λ/Δ_n (nanometer per refractive index (nm/RIU)), where Δ_λ is the shifting rate of the transmittance peak's resonant wavelength, while Δ_n denotes the refraction index's changing rate in the plasmonic based sensing structure [19].

The structural parameters of the proposed design under simulation, are set to $L_1 = 200\,\mathrm{nm}$, $L_2 = 120\,\mathrm{nm}$, $g = 10\,\mathrm{nm}$, and $D = 100\,\mathrm{nm}$, respectively. For initial calculations, the height between the hexagonal centers is taken as zero.

3. NUMERICAL RESULTS AND DISCUSSION

First, the transmission spectra and their corresponding resonance dips are simulated with the refractive index n set to be 1, and the results are depicted in Fig. 2(a), where it is noticed that the transmission

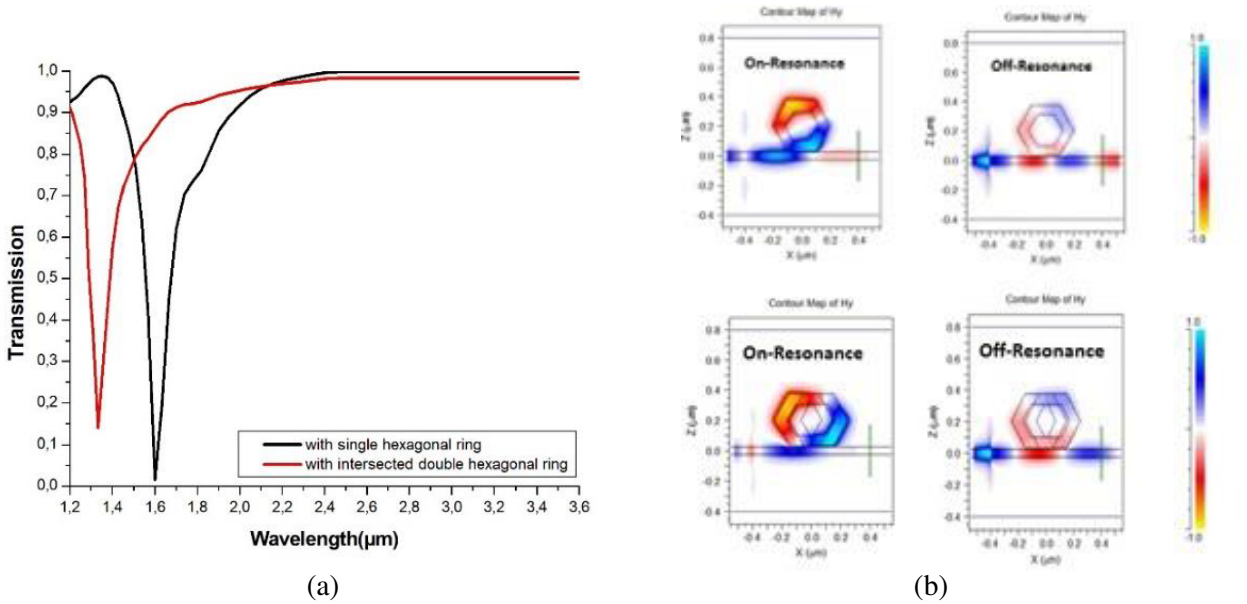

(a) (b)

Figure 2. (a) The transmission spectra and the magnetic filed H_y patterns of the MIM plasmonic structure with single hexagonal and with double hexagonal ring with $n = 1$, $L_1 = 200\,\text{nm}$, $L_2 = 120\,\text{nm}$, $g = 10\,\text{nm}$ and $D = 100\,\text{nm}$.

dip of the structure with the double hexagonal rings occurred at the resonance wavelength of 1.5989 μm, whereas in the case of the single hexagonal ring resonator, it occurred at 1.3317 μm, and their corresponding transmission levels were 98.5% and 86%, respectively. So, a red shift occurs in the structure with the double hexagonal shaped rings, alongside an improvement of 15% in the device's transmission.

Figure 2(b) depicts the magnetic field distribution patterns for both structures with single and double hexagonal ring resonator, where it is clearly noticed that the EM waves are transmitted and collected from both ends of the waveguide, when the operating wavelength is different from the resonator's one, as illustrated in mode off-resonance, where the operating wavelength was set to 1 μm. On the other hand, in the case when the operating wavelength and the resonator's one are the same (1.5989 μm), most of the energy is not transmitted as illustrated in mode on-resonance, due to the coupling between the double intersected hexagonal ring resonator and the waveguide, which prohibited the waves from transmitting to the other end, hence the sensors operation principle.

Same observations were noted from the obtained results for the proposed single hexagonal ring resonator structure, at 1 μm and 1.3317 μm of the resonance wavelength as illustrated in mode off-resonance and on-resonance, respectively.

Next, the refractive index n is varied from 1 to 1.2 in a step of 0.05, and the corresponding transmission spectra of both MIM based plasmonic waveguides coupled to double hexagonal ring resonator are illustrated in Fig. 3. It is clearly noticed that by increasing the refractive index n, a red-shift of resonance wavelength occurs (See Fig. 3(a)). This red-shift phenomenon is induced by the proportional relation between the $\text{Re}(n_{eff})$ and the wavelength λ_m, according to Eq. (2). The change in the resonant wavelength is produced by the refractive index shift Δn. From Fig. 3(b) we can see the linearity maintained relation between the resonance wavelengths of MIM based plasmonic waveguides (single and double hexagonal ring resonator) and the refractive indices. Also, to observe the influence of the refraction index on the design's sensitivity, all other structural parameters were maintained, and the refraction index n was adjusted from 1 to 1.2. As a consequence, the sensitivity was roughly 1700 and 1280 nm/RIU for the double hexagonal ring resonator structure and single hexagonal ring one, respectively. So, it is readily observed that the double hexagonal ring shape exhibited an improvement in the device's sensitivity by 33 percent.

By controlling the lateral coupling in the waveguide and resonator interface, one can improve the

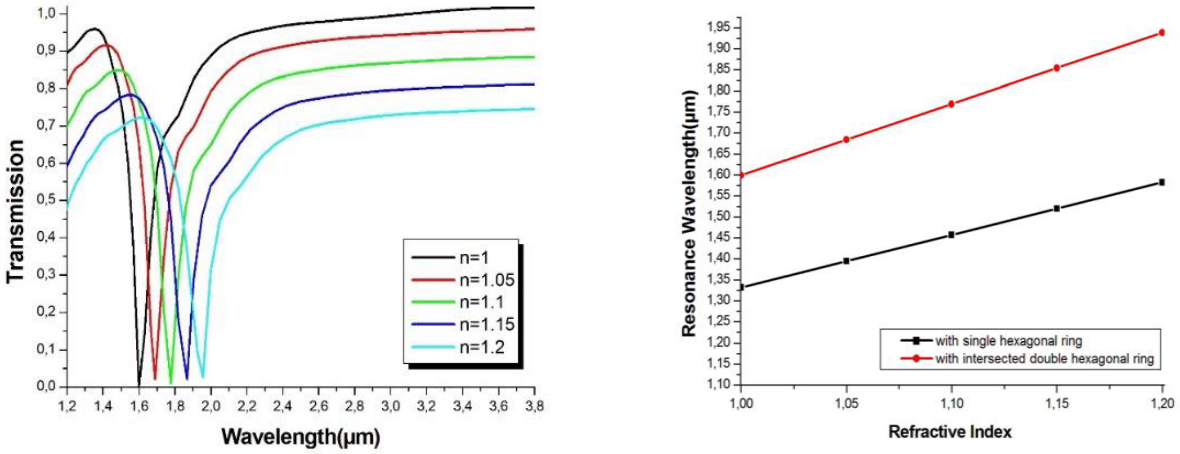

(a) (b)

Figure 3. (a) The transmission spectrum of the MIM waveguides coupled with double hexagonal ring for different refractive index n, (b) the resonance wavelength versus the refractive index n of the material under sensing.

coupling strength. Double intersected hexagonal ring-shaped resonators with a long length of interaction along the entire flat sidewalls of the resonator compared by single hexagonal are of high important effect. Therefore, they can facilitate the tight constraint on the gap separation between the resonator and the side-coupled waveguide effectively which makes sensing operation applicable.

To mimic the real characteristics of the proposed sensor, the refractive index of the glucose solution is described as [28]:

$$n = 0.00011889C + 1.33230545 \tag{3}$$

where C is the glucose content (g/L), and n is the refractive index of the glucose solution.

In order to investigate the relationship between the transmission spectrum and glucose concentration, using a sample with a concentration range of 0–200 g/L is considered in the resonator hexagonal ring. The resonance wavelength of the spectrum varies as the refractive index of the glucose solution in the sensor structure changes. Fig. 4(a) depicts the shift in the biosensor transmission spectrum for glucose concentrations ranging from 0 to 200 g/L. Fig. 4(a) shows that for every 50 g/L increase in glucose concentration, a 9.34 nm shift in the output resonance wavelength is estimated. The simulation results also reveal that the biosensor sensitivity for the sample with a glucose concentration in the range 0–200 g/L is equivalent to $S = 1670$ nm/RIU, which is consistent with the refractive index range of the sample: 1.3323–1.3561.

According to Fig. 4(b), this biosensor also exhibits a linear proportion with an increase in the glucose concentration range 0–200 g/L, suggesting that it might be utilized as a self-calibration sensor to determine various glucose concentrations.

The designed device is also appropriate to be used as a nanoscale temperature sensor, with a temperature adjustment method. A liquid, ethanol, with a high RI temperature coefficient (i.e., $dn/dT = 3.9410^{-4}$) can be injected into double hexagon-shaped rings cavities to act as a temperature sensor. Ethanol's RI can be defined as [29]:

$$n = 1.36048 - 3.94 \times 10^{-4}(T - T_0) \tag{4}$$

Here T_0 (room temperature) is tuned to 20°C [29], and T is the ambient temperature ranging from -100 to 60 degrees Celsius with a 40°C degree step. The linear relation between n and T is shown in Eq. (4). The temperature sensor's sensitivity is specified as $S_T = \Delta n/\Delta T$. Fig. 5(a) illustrates the transmittance spectrum of the proposed MIM plasmonic waveguide at various ambient temperatures (T), with the other parameters remaining unchanged from Fig. 2.

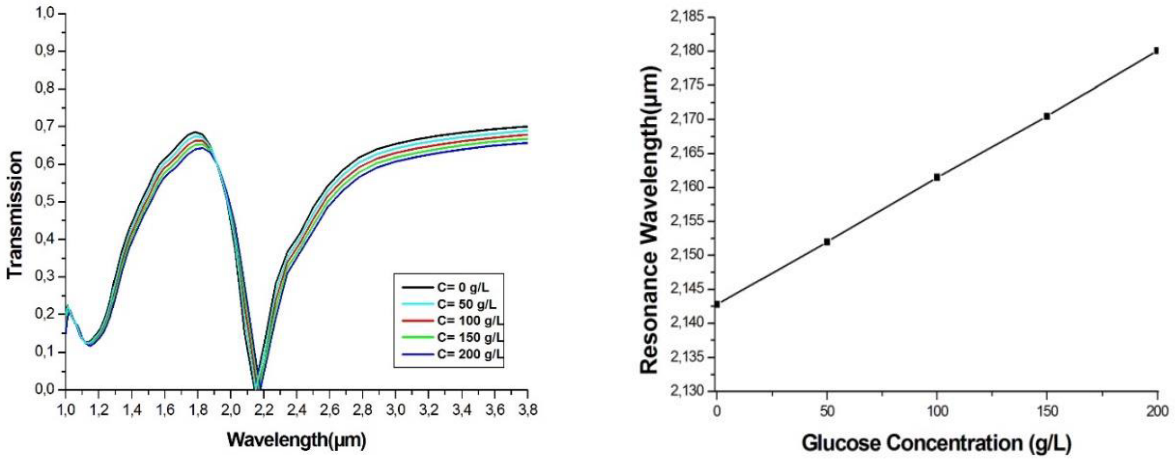

(a) (b)

Figure 4. (a) The transmission spectrum of the plasmonic sensor versus wavelength for different value of the glucose concentration at $L_1 = 200\,\text{nm}$, $L_2 = 120\,\text{nm}$, $g = 10\,\text{nm}$ and $D = 100\,\text{nm}$. (b) The resonance wavelength versus the glucose concentration.

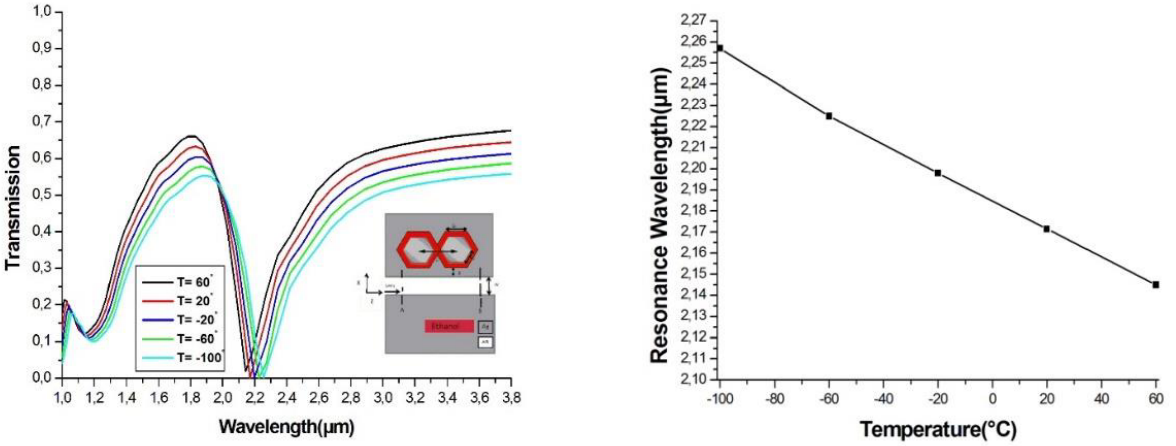

(a) (b)

Figure 5. (a) The transmission spectrum of the plasmonic sensor versus wavelength for different value of temperature at $L_1 = 200\,\text{nm}$, $L_2 = 120\,\text{nm}$, $g = 10\,\text{nm}$ and $D = 100\,\text{nm}$. (b) The resonance wavelength versus the temperature.

The peak shifts to shorter wavelengths (i.e., blueshift) when the temperature is raised from $-100°\text{C}$ to $60°\text{C}$ (in $40°\text{C}$ increments), as seen in Fig. 5(a). However, Fig. 5(b) shows a linear relationship between the positions of transmittance dips and temperature fluctuations. Furthermore, the sensor's temperature sensitivity can be calculated to be $0.685\,\text{nm}/°\text{C}$.

Furthermore, we will calculate and optimize the design's transmission and sensitivity by modifying the geometrical properties. First, the height H between the two hexagonal ring centers is investigated. The value of H fluctuates from 0 to 75 nm at 25 nm intervals, while the other parameters stay constant at $D = 100\,\text{nm}$, $g = 10\,\text{nm}$, $L_2 = 120\,\text{nm}$, $L_1 = 200\,\text{nm}$, and $n = 1$.

The greatest transmittance at the peak is influenced by the coupling intensity, which is regulated by the gap size g, as the peak resonance is formed by the coupling between the MIM waveguide and the plasmonic hexagonal cavity resonator. According to Fig. 6, the maximum transmittance at the peak improves as the height H lowers. As the height H decreases, the peak wavelength displays a minor red

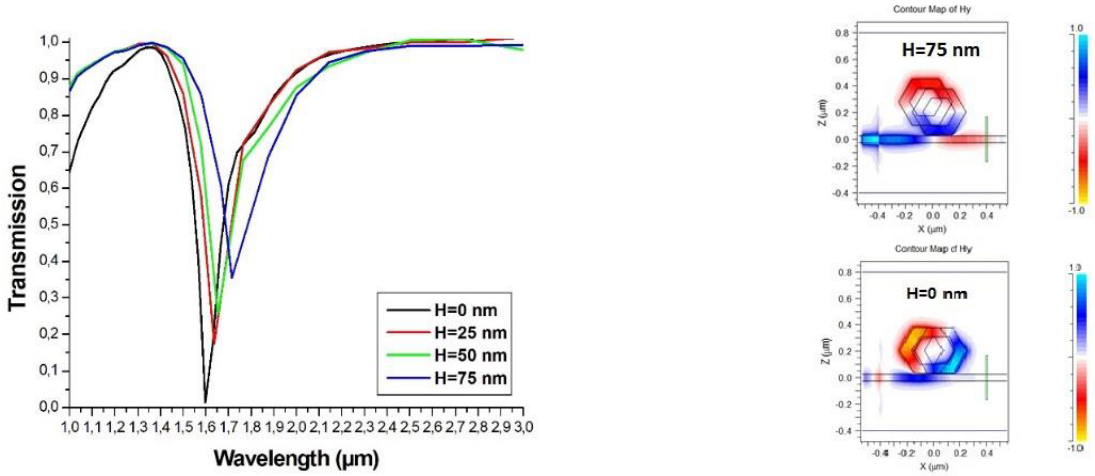

(a) (b)

Figure 6. Transmission spectra of the MIM waveguides coupled with double hexagonal ring cavities with changing H ($n = 1$, $L_1 = 200\,\text{nm}$, $L_2 = 120\,\text{nm}$, $g = 10\,\text{nm}$ and $D = 100\,\text{nm}$). The H_y field distribution is shown at the resonant peak for $H = 75\,\text{nm}$ and $H = 0\,\text{nm}$.

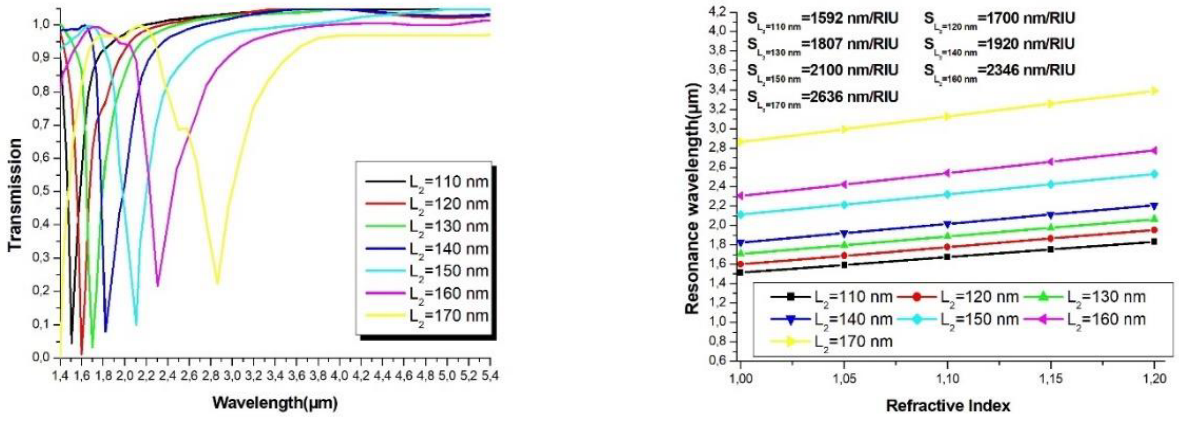

(a) (b)

Figure 7. (a) Transmission spectra of index 1 for L_2 varying from 110 to 170 nm. (b) The resonance wavelengths versus the refractive index for different L_2.

shift, which may be induced by a change in the effective index of the local SPP mode in the coupling zone. Fig. 6 displays the magnetic field distribution at the resonant peak for $H = 0\,\text{nm}$ and $H = 75\,\text{nm}$.

Secondly, in order to explore the influence of the inner side length on the sensor's performances, L_2 is altered from 110 to 170 nm in a step of 10 nm and displayed in Fig. 7. It can be shown that increasing L_2 causes an increase in resonance wavelength, i.e., a shift in resonance wavelength (see Fig. 7(a)), which can be described by Eq. (2): as L_2 grows, the propagation length of SPPs in the resonance cavity increases, causing the value of the resonant peak to increase. Also, it is seen that the linearity between the resonance wavelengths and the refractive indices is maintained, despite the variations in the value of L_2 as depicted in Fig. 7(b). More crucially, the bigger the value of L_2 (110 nm to 170 nm) is, the higher the sensor's sensitivity is, where the highest achievable one was at $L_2 = 170\,\text{nm}$ with a value of 2636 nm/RIU, i.e., a sensing resolution of 3.79×10^{-6} RIU, compared to a sensitivity of 1592 nm/RIU when L_2 was 110 nm. L_2 is set to the best obtained value of 170 nm for the next performance analysis.

Third, the effect of distance D on the MIM-based sensor is investigated by altering D from 100 to 250 nm in 50 nm increments with a refractive index $n = 1$. The corresponding transmission spectra

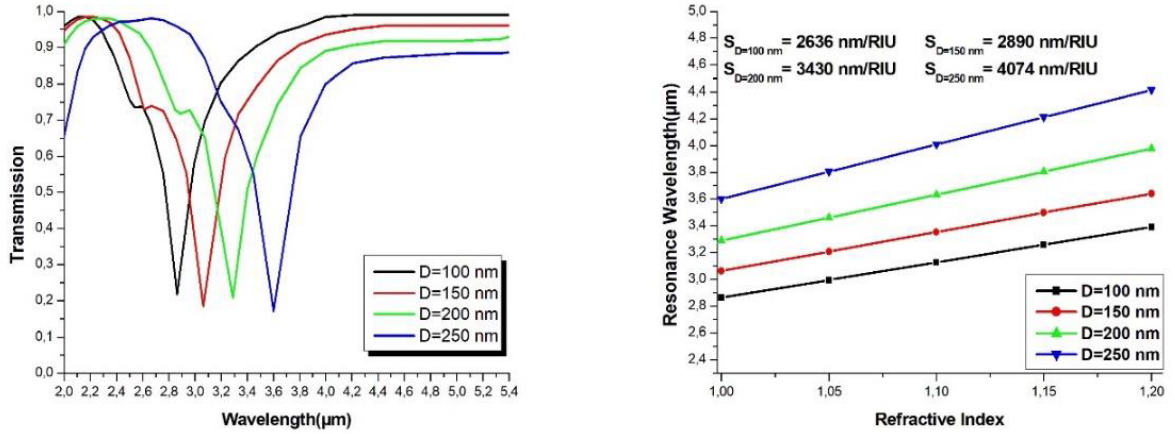

Figure 8. (a) Transmission spectra of index 1 for D varying from 100 to 250 nm. (b) The resonance wavelengths versus the refractive index for different D.

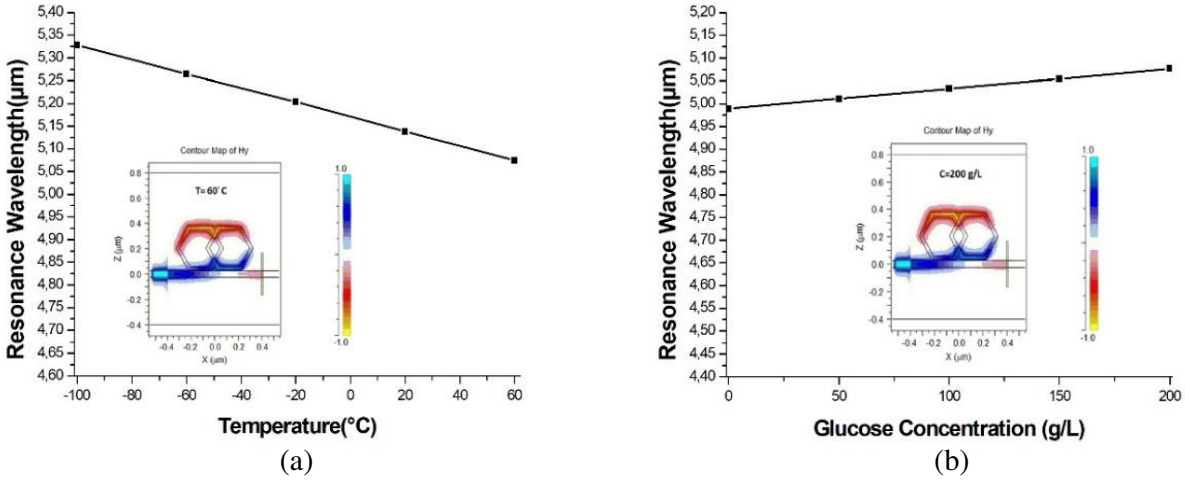

Figure 9. (a) The resonance wavelength versus the glucose concentration. (b) The resonance wavelength versus the temperature ($L_1 = 200$ nm, $L_2 = 170$ nm, $g = 10$ nm, $H = 0$ nm and $D = 250$ nm). The H_y field distribution is shown at the resonant peak for $C = 200$ g/L and $T = 60°$.

are displayed in Fig. 8(a), where it is evident that increasing the value of D induces a red shift in the resonance wavelength (we obtain three peaks in the MIR). The linearity between the wavelength and the refractive indices is maintained even when the value D is raised, as illustrated in Fig. 8(b).

Furthermore, the greater the value of D (from 100 to 250 nm) is, the better the sensor's sensitivity is, with the largest attainable sensitivity being 4074 nm/RIU, i.e., sensing resolution of 2.45×10^{-6} RIU, for $D = 250$ nm, compared to a sensitivity of 2636 nm/RIU for $D = 100$ nm.

Figure 9(a) illustrates a linear connection between the resonant wavelength peak and temperature fluctuations in the MIR. Additionally, the sensor's temperature sensitivity may be calculated to be 1.55 nm/°C. Fig. 9(b) indicates that this sensor has a linear relation with an increase in the glucose concentration range 0–200 g/L in the MIR band. Furthermore, the biosensor's sensitivity may be calculated as 3910 nm/RIU.

To emphasize the overall performance of our proposed structure, Table 1 compares the sensitivity (S) of several proven MIM plasmonic sensors in the published articles to ours.

Furthermore, we can use the previous articles to confirm that our proposed structure can be easily

Table 1. Sensitivity comparison of different sensor structures.

Reference/Application	Sensitivity S (nm/RIU) and S_T (nm/°C)	year
[30]/Temperature	$S = 1326$ and $S_T = 0.53$	2017
[31]/Temperature	$S = 2320$ and $S_T = 0.84$	2017
[32]/Temperature	$S = 1556$ and $S_T = 0.61$	2020
[33]/Glucose	$S = 1070$	2020
[34]/Glucose	$S = 1948.67$	2020
[31]/Glucose	$S = 2162$	2021
[35]/Glucose	$S = 1500$	2021
[32]/Temperature	$S = 2625.8$ and $S_T = 1.04$	2021
In this work: Main design	$S = 4074$	
For the Glucose	$S = 3910$	2022
For the temperature	$S_T = 1.55$	

manufactured in practice, and this design combines a simple design and rapid fabrication process. The parameters of the proposed sensor have been chosen considering 10 nm precision offered by the NIL (nanoimprint lithography) fabrication technique, which is less costly and capable of providing higher throughput than any other lithographic fabrication techniques such as EBL (electron beam lithography) and FIB (focused ion beam) [36]. The NIL method prints silver patterns on silicon wafer [37], then removes residual resin using O_2 plasma etching [38]. Using the electron beam, evaporation coats the silver layer upon the silicon wafer; next, the resin imprints will be removed, and cavities are formed in the lift-of process [39].

4. CONCLUSIONS

In this study, a highly sensitive refractive index sensor based on a MIM plasmonic device with intersecting double hexagonal shaped ring resonator, simulated and analyzed using the finite-difference time-domain (FDTD) approach included in the commercial simulator R-soft, is provided. The locations of the transmission peaks and dips may be adjusted by simply modifying both the inner side length and the distance between the centers of the double crossed hexagonal ring resonators. Moreover, these transmission peaks have a linear connection with the refractive index. Furthermore, our suggested MIM-based sensor has a superior sensitivity performance of $S = 4074$ nm/RIU, temperature sensitivity around 1.55 nm/°C, and optimum linear sensitivity of $S = 3910$ nm/RIU in 0–200 g/L glucose concentration, making it an appealing and potentially extremely sensitive refractive index-based nano-sensor.

REFERENCES

1. Ben Salah, H., A. Hocini, M. N. Temmar, and D. Khedrouche, "Design of mid infrared high sensitive metal-insulator-metal plasmonic sensor," *Chinese J. Phys.*, Vol. 61, 86–97, 2019.
2. Gramotnev, D. K. and I. B. Sergey, "Plasmonics beyond the difraction limit," *Nature Photonics*, Vol. 4, No. 2, 83–91, 2010.
3. Bahri, H., S. Mouetsi, A. Hocini, and H. Ben Salah, "A high sensitive sensor using MIM waveguide coupled with a rectangular cavity with Fano resonance," *Opt. Quant. Electron.*, Vol. 53, 332, 2021.
4. Tavousi, A., M. A. Mansouri-Birjandi, and M. Janfaza, "Graphene nanoribbon assisted refractometer based biosensor for mid-infrared label-free analysis," *Plasmonics*, Vol. 14, No. 5, 1207–1217, 2019.

5. Huang, Z., L. Wang, B. Sun, M. He, J. Liu, H. Li, and X. Zhai, "A mid-infrared fast-tunable graphene ring resonator based on guided-plasmonic wave resonance on a curved graphene surface," *Journal of Optics*, Vol. 16, No. 10, 105004, 2014.
6. Han, Z., L. Liu, and Erik, "Ultra-compact directional couplers and Mach Zehnder interferometers employing surface plasmon polaritons," *Optics Communications*, Vol. 259, No. 2, 690–695, 2006.
7. Fang, Z., Y. Wang, A. E. Schlather, Z. Liu, P. M. Ajayan, G. de Abajo, F. Javier, P. Nordlander, X. Zhu, and N. J. Halas, "Active tunable absorption enhancement with graphene nanodisk arrays," *Nano Letters*, Vol. 14, No. 1, 299–304, 2014.
8. Gomez, D., S. Juan, and P. Julien, "Graphene-based plasmonic switches at near infrared frequencies," *Optics Express*, Vol. 21, No. 13, 15490–15504, 2013.
9. Sadeghi, T., T. G. Saeed, and B. Hamed, "Improving the performance of nanostructure multifunctional graphene plasmonic logic gates utilizing coupled-mode theory," *Applied Physics B*, Vol. 125, No. 10, 189, 2019.
10. Dolatabady, A. and G. Nosrat, "All-optical logic gates in plasmonic metal-insulator-metal nanowaveguide with slot cavity resonator," *Journal of Nanophotonics*, Vol. 11, No. 2, 026001, 2017.
11. Madadi, Z., K. Abedi, G. Darvish, and M. Khatir, "An infrared narrow-band plasmonic perfect absorber as a sensor," *Optik*, Vol. 183, 670–676, 2019.
12. Ben Salah, H., A. Hocini, H. Bahri, and N. Melouki, "High sensitivity plasmonic sensor based on metal-insulator-metal waveguide coupled with a notched hexagonal ring resonator and a stub," *ECS Journal of Solid State Science and Technology*, Vol. 10, No. 8, 081001, 2021.
13. Soref, R., "Mid-infrared photonics in silicon and germanium," *Nature Photonics*, Vol. 4, No. 8, 495–497, 2010.
14. Singh, V., L. T. Pao, P. Neil, and L. Hongtao, "Mid-infrared materials and devices on a Si platform for optical sensing," *Science and Technology of Advanced Materials*, Vol. 15, 014603, 2014.
15. Hodgkinson, J. and R. P. Tatam, "Optical gas sensing: A review," *Measurement Science and Technology*, Vol. 24, No. 1, 012004, 2012.
16. El Shamy, R. S., D. Khalil, and M. A. Swillam, "Mid infrared optical gas sensor using plasmonic Mach-Zehnder interferometer," *Sci. Rep.*, Vol. 10, 1293, 2020.
17. Sharif, M. and A. Swillam, "Metal-Less silicon plasmonic mid-infrared gas sensor," *Journal of Nanophotonics*, Vol. 10, No. 2, 026025, 2016.
18. Wang, G., H. Lu, X. Liu, Y. Gong, and L. Wang, "Optical bistability in metal-insulator-metal plasmonic waveguide with nanodisk resonator containing Kerr nonlinear medium," *Applied Optics*, Vol. 50, No. 27, 5287–5290, 2011.
19. Wu, T. S., Y. M. Liu, Z. Y. Yu, Y. W. Peng, C. G. Shu, and H. Ye, "The sensing characteristics of plasmonic waveguide with a ring resonator," *Opt. Express*, Vol. 22, No. 7, 7669–7677, 2014.
20. Rakhshani, M. R., "Refractive index sensor based on concentric triple racetrack resonators side coupled to metal-insulator-metal waveguide for glucose sensing," *Journal of the Optical Society of America B*, Vol. 36, No. 10, 2834–2842, 2019.
21. Shi, H., S. Yan, X. Yang, X. Wu, W. Wu, and E. Hua, "A nanosensor based on a metal-insulator-metal bus waveguide with a stub coupled with a racetrack ring resonator," *Micromachines*, Vol. 12, No. 5, 495, 2021.
22. Chou Chau, Y. F., C. T. Chou Chao, H. J. Huang, N. T. Kumaran, C. M. Lim, and H. P. Chiang, "Ultra-high refractive index sensing structure based on a metal-insulator-metal waveguide-coupled T-shape cavity with metal nanorod defects," *Nanomaterials*, Vol. 9, 1433, 2019.
23. Chou Chau, Y. F., "Mid-infrared sensing properties of a plasmonic metal-insulator-metal waveguide with a single stub including defects," *J. Phys. D: Appl. Phys.*, Vol. 53, 11, 2020.
24. Taflove, A. and S. C. Hagness, *Computational Electrodynamics: The Finite-Difference Time-Domain Method*, 3rd Edition, Artech House, Boston, MA, USA, 2005.
25. Zafar, R. and M. Salim, "Enhanced figure of merit in Fano resonance-based plasmonic refractive index sensor," *IEEE Sensors Journal*, Vol. 15, No. 11, 6313–6317, 2015.

26. Xie, Y., Y. Huang, W. Zhao, W. Xu, and C. He, "A novel plasmonic sensor based on metal-insulator-metal waveguide with side-coupled hexagonal cavity," *IEEE Photonics Journal*, Vol. 7, No. 2, 1–12, 2015.
27. Hocini, A., H. Ben Salah, D. Khedrouche, and N. Melouki, "A high-sensitive sensor and band-stop filter based on intersected double ring resonators in metal-insulator-metal structure," *Optical and Quantum Electronics*, Vol. 52, 336–345, 2020.
28. Areed, N. F., M. F. O. Hameed, and S. S. A. Obayya, "Highly sensitive face-shaped label-free photonic crystal refractometer for glucose concentration monitoring," *Opt. Quant. Electron.*, Vol. 49, 1–12, 2017.
29. Sagor, R. H., M. F. Hassan, A. A. Yaseer, E. Surid, and M. I. Ahmed, "Highly sensitive refractive index sensor optimized for blood group sensing utilizing the Fano resonance," *Appl. Nanosci.*, Vol. 11, 521–534, 2021.
30. Jubayer, M. A., H. Rakib, and M. I. Zahurul, "Numerical studies on a plasmonic temperature nanosensor based on a metal-insulator-metal ring resonator structure for optical integrated circuit applications," *Photonics and Nanostructures — Fundamentals and Applications*, Vol. 25, 52–57, 2017.
31. Rakhshani, M. and M. Mansouri-Birjandi, "High sensitivity plasmonic refractive index sensing and its application for human blood group identification," *Sens. Act. B: Chem.*, Vol. 249, 168–176, 2017.
32. Sagor, R., M. Hassan, S. Sharmin, T. Adry, and M. Emon, "Numerical investigation of an optimized plasmonic on-chip refractive index sensor for temperature and blood group detection," *Results Phys.*, Vol. 19, 2020.
33. Hassan, M. F., I. Tathfif, M. Radoan, and R. H. Sagor, "A concentric double-ring resonator based plasmonic refractive index sensor with glucose sensing capability," *2020 IEEE Reg. 10 Conf.*, 91–96, 2020.
34. Butt, M. A., N. L. Kazanskiy, and S. N. Khonina, "Highly integrated plasmonic sensor design for the simultaneous detection of multiple analytes," *Curr. Appl. Phys.*, Vol. 20, 1274–1280, 2020.
35. Chou Chau, Y. F., "Multiple-mode bowtie cavities for refractive index and glucose sensors working in visible and near-infrared wavelength range," *Res. Sq.*, 1–25, 2021.
36. Jung, W. K. and K. M. Byun, "Fabrication of nanoscale plasmonic structures and their applications to photonic devices and biosensors," *Biomed. Eng. Lett.*, Vol. 1, 153–162, 2011.
37. Lee, F. Y., K. H. Fung, T. L. Tang, W. Y. Tam, and C. T. Chan, "Fabrication of gold nano-particle arrays using two-dimensional templates from holographic lithography," *Curr. Appl. Phys.*, Vol. 9, 820–825, 2009, https://doi.org/10.1016/j.cap.2008.07.017.
38. López-Muñoz, G. A., M. C. Estevez, E. C. Peláez-Gutierrez, A. Homs-Corbera, M. C. García-Hernandez, J. I. Imbaud, and L. M. Lechuga, "A label-free nanostructured plasmonic biosensor based on Blu-ray discs with integrated microfluidics for sensitive biodetection," *Biosens. Bioelectron.*, Vol. 96, 260–267, 2017, https://doi.org/10.1016/j.bios.2017.05.020.
39. Kazanskiy, N. L., M. A. Butt, and S. N. Khonina, "Nanodots decorated MIM semi-ring resonator cavity for biochemical sensingapplications," *Photonics Nanostructures — Fundam. Appl.*, Vol. 42, 100836, 2020, https://doi.org/10.1016/j.photonics.2020.100836.